CHARACTERIZATION OF UNSTEADY FLOW STRUCTURES NEAR LEADING-EDGE SLAT: PART I. PIV MEASUREMENTS

Luther N. Jenkins*, Mehdi R. Khorrami†, and Meelan Choudhari†
NASA Langley Research Center, Hampton, Virginia, 23681

A comprehensive computational and experimental study has been performed at the NASA Langley Research Center as part of the Quiet Aircraft Technology (QAT) Program to investigate the unsteady flow near a leading-edge slat of a two-dimensional, high-lift system. This paper focuses on the experimental effort conducted in the NASA Langley Basic Aerodynamics Research Tunnel (BART) where Particle Image Velocimetry (PIV) data was acquired in the slat cove and at the slat trailing edge of a three-element, high-lift model at 4, 6, and 8 degrees angle of attack and a freestream Mach Number of 0.17. Instantaneous velocities obtained from PIV images are used to obtain mean and fluctuating components of velocity and vorticity. The data show the recirculation in the cove, reattachment of the shear layer on the slat lower surface, and discrete vortical structures within the shear layer emanating from the slat cusp and slat trailing edge. Detailed measurements are used to examine the shear layer formation at the slat cusp, vortex shedding at the slat trailing edge, and convection of vortical structures through the slat gap. Selected results are discussed and compared with unsteady, Reynolds-Averaged Navier-Stokes (URANS) computations for the same configuration in a companion paper by Khorrami, Choudhari, and Jenkins (2004). The experimental dataset provides essential flow-field information for the validation of near-field inputs to noise prediction tools.

Nomenclature

C	=	chord, 0.457 meters
C_P	=	pressure coefficient, $\frac{p - p_\infty}{q_\infty}$
d	=	distance along survey line near slat cusp, meters
p	=	pressure measured along model surface, Pa
p_∞	=	freestream static pressure, Pa
q_∞	=	freestream dynamic pressure, Pa
TKE	=	turbulent kinetic energy, $(m/s)^2$
U	=	streamwise velocity component, m/s
U_∞	=	freestream velocity, m/s
V	=	vertical velocity component, m/s
V_{mag}	=	velocity magnitude, m/s
X	=	streamwise coordinate, mm
Y	=	vertical coordinate, mm
ω_Z	=	spanwise vorticity component, s^{-1}
α	=	angle of attack, degrees

I. Introduction

PREDICTION, control, and mitigation of airframe noise require a thorough understanding of the flow physics and underlying noise mechanisms. This is especially true when using computational methods to predict and

* Research Engineer, Flow Physics and Control Branch, Mail Stop 454.
† Research Engineer, Computational Modeling and Simulation Branch, Mail Stop 128, Associate Fellow, AIAA.

assess noise levels associated with high-lift systems. Computational studies on high-lift systems by Khorrami, et al.[1] and Choudhari, et al.[2] have shown the relationship between large-scale flow fluctuations in the near-field and measured far-field noise. Their findings suggest that improper modeling of the unsteady flow structure can significantly affect the accuracy of calculations used for airframe noise prediction and assessment, thus emphasizing the importance of validating computational methods. Validation is typically accomplished through detailed comparisons with wind tunnel or flight data. Although acoustic datasets are readily available to validate sound pressure levels and signatures, the number of datasets containing unsteady flow-field information is limited and prevents the direct validation of a key input to the noise prediction process.

This is especially true for the region near a leading-edge slat, which has been identified as a source of both tonal and broadband noise. While the aerodynamic performance enhancements associated with the slat have been studied extensively, questions about the detailed structure of the slat cove flow and its impact on far field noise still remain. The flow structure in the slat cove is extremely complex and its characteristics depend on geometry, air speed, angle of attack, slat deflection angle, slat gap, and overlap. While designed to blend into the main element and eliminate potential surface discontinuities in the stowed configuration, the deployed slat exposes the cusp and trailing edge to the flow, resulting in a region of separated flow along the slat pressure surface. The separated flow generates instabilities and convects vorticity that can then interact with nearby surfaces to generate noise.

Techniques for capturing the details of this process and model installation considerations present a challenge to experimentalists. Wind tunnel models of high-lift systems usually require some type of bracket to attach the slat and the flap to the main element. In some cases, bracket size and attachment points required to withstand the flow-induced forces produced at large deflection angles limit physical and optical access to the slat cove. In addition to model installation issues, experimentalists must also select the appropriate measurement technique to resolve the unsteady flow field, including free shear layers and flow reversal. Many researchers[3-8] have used hot-wire anemometry (HWA) to survey the near wake behind the slat trailing edge to obtain velocity profiles, measure shedding frequencies, and identify potential "noise producing" structures passing through the slat gap. Hot-wire anemometry is well-suited to investigate shear layers and provides valuable information about the time-dependent characteristics of the flow field; but unfortunately, traversing a hot-wire probe within the confines of a slat cove can be problematic. Alternatively, non-intrusive measurement techniques such as Laser Doppler Velocimetry (LDV), Laser-Induced Thermal Acoustics (LITA), and Particle Image Velocimetry (PIV) have proven to be effective tools to obtain flow-field information and details about the flow structure associated with high-lift wing configurations. To date, these techniques have been used primarily to investigate trailing-edge wakes, confluent boundary layers, and flow around flap side edges, but they have also proven effective in measuring the flow field in the slat cove. PIV has been used by Moriarty and Heinreck[9] to examine the effect of Mach number and slat deflection angle on the flow field within the cove of a three-element wing with a full-span slat and part-span flap. Their results show the mean flow structure in the cove for slat deflection angles of 5 degrees and 25 degrees and the high turbulence levels associated with the shear layer and its reattachment. Takeda, et al.[10,11] used LDV, PIV, and HWA to characterize the slat cove flow field on a three-element configuration with the slat deflected at 25 degrees. Like Moriarty, their results showed high turbulence levels near reattachment, but they also identified coherent structures (rollers) in the shear layer originating at the slat cusp, large vortical structures passing through the slat gap, and shedding from the slat trailing edge. Despite the quality of these datasets, differences in model geometry between these experiments and the calculations of References 1 and 2 only permit qualitative comparisons between the measured data and the computed flow field.

The purpose of the present investigation was to explore the unsteady flow field in the slat cove of a high-lift configuration by measuring the 2D, instantaneous velocity field using PIV. The resulting data and analysis are used to further characterize the flow physics associated with the slat cove region and to establish a comprehensive dataset for the validation of time-accurate computations. A companion paper by Khorrami, Choudhari, and Jenkins[12] describes the computational part of this study and presents detailed comparisons between the experimental and computational results. This paper outlines the details of the experiment and discusses the various flow features associated with the flow field in the slat cove.

II. Experimental Apparatus and Methods

A. Test Facility

The experiment was conducted in the NASA-Langley Basic Aerodynamics Research Tunnel (BART). The BART is a subsonic, atmospheric wind tunnel used to investigate the fundamental characteristics of complex flow fields and to acquire detailed data for the development and validation of CFD models and methods. The tunnel has a closed test section with a height of 0.711 meters, a width of 1.016 meters, and a length of 3.048 meters. The maximum velocity at the test section entrance is approximately 56 m/s and the turbulence level is 0.09%. This velocity equates to a Mach Number of 0.17 and a unit Reynolds Number (Re/m) of 3.64 million. Additional information about the BART can be found in References 13, 14, and 15.

B. Model

Measurements were performed on a McDonnell Douglas Aerospace (now Boeing) 30P30N, high-lift configuration. Geometrical settings associated with this configuration are listed in Table 1. This particular geometry has been used in studies by Klausmeyer[16] to examine separation control using micro-vortex generators on the flap and by Paschal[17] to characterize unsteadiness in the slat wake. The model, shown in Figure 1, has a nested chord of 0.457 meters and consists of a main element, slat, and single element flap that span the tunnel width. The slat chord and flap chord are 15% and 30% of the stowed chord, respectively. The slat cusp and trailing edge are small but have finite thickness. Figure 1 shows the dowel/slip bearing and turntable used to support the model and attach it to the tunnel side walls. A computer-driven actuator rotated the turntable to set angle of attack. Brackets attach the slat and flap to the main element and are used to set the gap, overhang, and deflection angles. In previous tests using this model, more than half of the slat cove was obscured by the brackets; so, for this investigation, the model was modified as shown in Figure 2 to include a "J-bracket". The "J-bracket" provided full optical access into the cove and the necessary strength to withstand the aerodynamic loads. It was decided to install the brackets on the pressure side of the model to minimize their potential effect on the upper surface flow.

Slat angle, δ_s	30°
Flap angle, δ_f	30°
Slat Gap, g_s	2.95%
Flap Gap, g_f	1.27%
Slat Overhang, o_s	-2.5%
Flap Overhang, o_f	0.25%

Table 1: Geometrical Settings

The model was instrumented with a single chordwise row of pressure orifices on the centerline of the three elements and a single spanwise row of pressure orifices on both the main element and flap. Unlike Reference 17, sidewall blowing was not used; however, the pressures measured by the spanwise rows verified the quasi-two-dimensionality of the flow in the measurement region. The flow on the surface was allowed to transition naturally.

C. Data Acquisition

Flow-field velocity measurements were made using a 2D, Digital Particle Image Velocimetry (DPIV) system, which consisted of a single, high-resolution, video camera with a sensor size of 1360 pixels by 1024 pixels. The camera was mounted to a traverse system surrounding the tunnel along with the laser and light-sheet optics. A 1.5 mm thick light sheet was generated using a pulsed, frequency-doubled, 200mJ Nd-YAG laser operated at 5 Hz. The light sheet was aligned perpendicular to the model surface and parallel to the model centerline. The relative location of the measurement areas with respect to leading edge of the main element are shown in Figure 3. These planes are located 101.6 mm from the model centerline in the spanwise direction where the model was coated with a fluorescent paper. The paper was measured to be 0.127 mm and was used to reduce the amount of laser light scattered from the surface. Images were acquired using 50 mm and 105 mm lenses, hereafter referred to as *PIV Setup I* and *PIV Setup II*. The longer focal length lens was used with *PIV Setup II* to provide better resolution near the slat cusp and trailing edge. The field of view, interrogation area, resulting measurement volume, and estimated uncertainty for the two PIV setups are summarized in Table 2.

PIV Configuration	Lens Focal Length	Field of View	Interrogation Area	Measurement Volume	Velocity Uncertainty
PIV Setup 1	50 mm	80 mm x 60 mm	32 pixels^2	1.88 mm^2	±1.18 m/s
PIV Setup 2	105 mm	30 mm x 20 mm	24 pixels^2	0.53 mm^2	±1.53 m/s

Table 2: PIV system parameters.

Data were acquired at 4, 6, and 8 degrees angle of attack and a tunnel speed of Mach = 0.17, which corresponds to a Reynolds Number based on the stowed chord of 1.7×10^6. The slat and gap settings were fixed throughout the test. To obtain sufficient seed density in the cove region, the entire room housing the tunnel was seeded with 4.0 micron particles produced by a theatrical fog machine. Each acquisition sequence consisted of a minimum of 400 image pairs that were processed using a 50% interrogation window overlap and the algorithm described in Reference 18 to obtain instantaneous velocities. The instantaneous velocities were then used to compute instantaneous vorticity and mean flow quantities. Estimation of the spanwise vorticity component, ω_Z, was accomplished using the method described in Reference 19. Subsets of the total number of image pairs were processed and the mean quantities were examined along a profile through the shear layer to verify statistical convergence.

III. Discussion of Results

In this presentation and discussion of results, the stowed model chord, C = 0.457 meters, has been used to normalize all distance quantities and the freestream velocity, U_∞ = 56 m/sec, has been used to normalize all quantities involving velocity. All distances and velocities are in the tunnel coordinate system. With the exception of the surface pressures and data acquired near the trailing edge, all distances are relative to the slat cusp.

A. Slat Cove Flow Field – General Description

1. Surface Pressure Distribution

Figure 4 shows surface pressures plotted with respect to model coordinates for the deployed configuration. The pressure distribution on the flap shows little variation among the three angles of attack, but as expected, the loading on the main element and slat increase with angle of attack. On the main element, increased loading at higher angles of attack is commensurate with higher suction due to the acceleration of the flow through the slat gap. On the slat, the favorable pressure gradient on both sides of the stagnation has implications on the boundary layer state and separation. According to Olson[6], the favorable pressure gradient contributes to a thinner boundary layer on the slat upper surface that leads to shedding at the trailing edge. Near the slat cusp, the favorable pressure gradient accelerates and energizes the flow, which influences the strength of the shear layer.

2. Mean Flow Field

Figures 5-7 show contours of the mean streamwise (U) and vertical (V) velocity in the cove for each angle of attack. The contours show regions of high negative velocity near the slat lower surface and slow moving fluid associated with recirculation. The streamwise velocity is highest near the slat cusp whereas the vertical velocity reaches its maximum value near the slat gap. The Mach number in this region is estimated to be 0.26. Compared to the other angles, α=4° has the largest recirculation region in terms of streamwise extent and higher negative velocity in the region between Y/C=0.05 and Y/C=0.09. This negative velocity is associated with the main element, and although its magnitude is only 16 percent of the freestream velocity, it influences the shear layer trajectory in the vicinity of the reattachment point more than at the other angles of attack. This effect can be seen in Figures 8-10 where the streamlines between Y/C = 0.06 and Y/C = 0.10 at α=4° are almost vertical compared to the other angles. The streamlines were also used to estimate the average distance along the slat lower surface between the reattachment point and the slat trailing edge. These distances were estimated to be 6.77 mm at α=4°, 8.54 mm at α=6°, and 10.93 mm at α=8°. The proximity of the mean reattachment point to the slat trailing edge at α=4° and the inherent unsteadiness of the shear layer may account for the random ejection of vortices through the slat gap as seen in prior experiments[17].

Figures 11-13 show contours of the mean spanwise vorticity and turbulent kinetic energy (TKE). The turbulent kinetic energy was estimated using two components of the fluctuating velocity field. Although this is not equivalent to the true turbulent kinetic energy, Moriarty[9] has shown this to be a useful quantity for comparisons. The contours

show a well-defined shear layer in all three cases with comparable levels of vorticity except near the slat cusp. In this region, the vorticity levels decrease with increasing angle of attack and are due to differences in flow velocity. The shear layer thickness is nearly the same for all of the angles except in the reattachment region. Reattachment produces large velocity fluctuations as reflected in the turbulent kinetic energy contours, initiates the interaction of vorticity with the surface, and distributes the vorticity over the slat lower surface where it is either entrained into the recirculation region or ejected through the slat gap. Simulations by Khorrami[12] have identified the reattachment region as the source of low frequency waves that can radiate away from the slat. Indeed, the contours show that the highest levels of turbulent kinetic energy occur near reattachment and that the spatial extent of the turbulent region increases as the angle of attack decreases. Although more in depth study is needed, the higher broad-band noise associated with low angles of attack may be coupled with the expanse of this region. Although entrainment of shear layer structures within the recirculation region is evident at each angle, the vorticity levels in the recirculation region are not significant when compared to those in the shear layer.

3. Instantaneous Flow Field

To examine the unsteady flow structure, individual frames were selected from the PIV data at each angle to produce contours of instantaneous spanwise vorticity shown in Figures 14-16. The contours highlight the co-rotating vortices with positive sign formed at the slat cusp and show their convection towards the slat lower surface. A visual inspection of a series of individual frames revealed two apparent states for the unsteady flow field in the slat cove. Cove State 1 is shown in Figures 14a, 15a, and 16a and is characterized by the formation of vortices at the slat cusp and their subsequent convection towards the slat lower surface within the shear layer. As the shear layer reattaches, some of the vortices are entrained into the recirculation region where they diffuse and some are carried through the slat gap. The entrainment is more evident at α=4° which may be due to the angle at which the shear layer reattaches on the slat lower surface (Fig. 8). The streamlines in Figures 9 and 10 indicate that the angle at which the shear layer approaches the slat lower surface is more acute at α=6° and α=8° than at α=4°. This flow state gives the vortices greater opportunity to interact with the slat lower surface, although it is not clear whether or not (or how much) this would contribute to higher sound pressure levels for the noise radiated from this location. Cove Flow State 2 is depicted in Figures 14b, 15b, and 16b and shows vortices approaching the slat lower surface with little, if any, entrainment. Instead, vortices are convected towards the slat trailing edge where they interact with the surface.

B. Flow Details Near Slat Cusp

To examine the shear layer formation and its interaction with the recirculation region in greater detail, the laser light sheet was projected through the slat gap into the cove region from above the model and PIV images were acquired near the slat cusp using *PIV Setup II*. For this discussion, data from the mean flow field was interpolated onto a line perpendicular to the slat cusp, hereafter referred to as the "survey line" and shown in Figure 17. Velocity magnitudes computed along the survey line using two velocity components are compared in Figure 18. The variable on the abscissa is the normalized distance along the survey line and the dotted line denotes the location of the slat cusp with respect to the profile. The profiles clearly show a significant velocity gradient between the cove and the outer flow. In fact, the velocity magnitude increases from less than 10% to as much as 120% of the freestream velocity. The velocities outside the shear layer between d/C = 0.002 and d/C = 0.004 are consistent with the surface pressures which showed a more favorable pressure gradient upstream of the cusp at α=4°. In Figure 19, profiles of spanwise vorticity show that the shear layer thickness remains constant over this angle of attack range despite some differences in peak vorticity and its location relative to the slat cusp.

Details about the shear layer formation and development are shown in Figures 20-22. Contours of instantaneous spanwise vorticity reveal elongated vortices with positive sign being shed at the slat cusp and then evolving into a stream of discrete, co-rotating vortices. Computer simulations by Khorrami, et al.[12] predict a vortex chain emanating from the slat cusp but also show vortices of negative sign, larger diameter, and significant strength adjacent to slat lower surface near the cusp. The simulations suggest that these vortices build up and eventually perturb the shear layer in the early stages of its formation. Inspection of a series of frames in addition to those presented here did reveal some negative sign vortices within the recirculation region but not in the region of the slat cusp. It should be noted that viewing the frames of spanwise vorticity in succession showed some unsteadiness in the shear layer near the cusp but additional work is needed to determine its implications to the slat cove flow field.

C. Flow Details Near Slat Trailing Edge

Based on prior studies[17], the same setup described in Section B was used to examine the flow in the vicinity of the slat trailing edge to capture the vortices passing through the slat gap. The contours in Figures 23-25 compare the instantaneous spanwise vorticity for $\alpha=4°$ and $\alpha=8°$ and are representative of the types of frames seen throughout the data acquired at this location. Similar to the cove flow, these results suggest that the flow near the slat trailing edge can be characterized or described by three possible states.

1. Slat State 1: Two-sided Shedding

This state, shown in Figures 23a and 23b, is characterized by classic shedding of negative and positive sign vortices from the slat trailing edge. The vortices are symmetric and begin to weaken 0.03 chord lengths downstream. The contours show no evidence of vortices passing through the slat gap.

2. Slat State 2: Two-sided Shedding and Ejection Through Slat Gap

This state, shown in Figures 24a and 24b, is characterized by vortex shedding as well as the emergence of discrete vortices of positive sign from the slat cove. The vortices are convected downstream adjacent to the shear layer originating at the slat trailing edge.

3. Slat State 3: One-sided Shedding and Ejection Through Slat Gap

This state, shown in Figures 25a and 25b, is characterized by the shedding of negative sign vortices from the slat trailing edge and the ejection of vortices of positive sign from the slat cove through the slat gap. Compared to $\alpha=8°$, the vortices ejected through the slat gap at $\alpha=4°$ are stronger, more distorted, and have a greater effect on the position of the shear layer originating at the slat trailing edge.

For the sample of frames inspected to characterize these states, it was noted that at $\alpha=4°$, the flow appeared to be in Slat States 2 and 3 in the majority of the frames, whereas at $\alpha=8°$, the three flow states were equally represented among the number of frames. It is believed that Slat States 1 and 2 coincide with Cove State 1 described in Section A-3 where the flow reattaches and travels along the slat lower surface for a short distance before reaching the slat trailing edge. Slat State 3 is believed to coincide with Cove State 2 where the flow reattaches close to the slat trailing edge. In some cases, the presence of vortices near the trailing edge may disrupt the flow adjacent to the slat lower surface causing the shedding at the slat trailing edge to become one-sided. Figures 26 and 27 show the position of the streamline from the slat trailing edge coinciding with the three flow states. In States 1 and 2, the streamline from the slat trailing edge stays in the same position; however, in State 3, the streamline moves closer to the main element giving the vortices that pass through the gap a greater opportunity to interact with the main element. Undoubtedly, simultaneous flow-field measurements in the slat cove and at the slat trailing edge are necessary to provide more specific details concerning these flow states.

IV. Conclusion

A comprehensive experimental and computational study has been conducted to characterize and understand the unsteady structures in the slat cove region of a high-lift system. Instantaneous velocities obtained from PIV images were used to examine the mean and instantaneous flow structure in the slat cove and also at the slat trailing edge at $\alpha=4°$, $\alpha=6°$, and $\alpha=8°$. The data show the recirculation in the cove, reattachment of the shear layer on the slat lower surface, discrete co-rotating vortices within the shear layer emanating from the slat cusp, and vortex shedding from slat trailing edge. The instantaneous spanwise vorticity was used to identify the following flow states associated with the shear layer in the slat cove and vortex shedding at the trailing edge:

<u>Cove</u>

- Cove State 1: Vortices convected from slat cusp towards the slat lower surface. At reattachment, some vortices are entrained into the recirculation region where they diffuse and some pass through the slat gap.
- Cove State 2: Vortices convected from slat cusp towards the slat lower surface. At reattachment, little entrainment occurs and most of the vortices interact with the trailing edge as they pass through the slat gap.

Slat Trailing Edge

- Slat State 1: Classic shedding of negative and positive sign vortices from the slat trailing edge. No evidence of vortices passing through the slat gap.
- Slat State 2: Vortex shedding and ejection of discrete vortices of positive sign from the slat cove.
- Slat State 3: Shedding of negative sign vortices from the slat trailing edge and the ejection of positive sign vorticity from the slat cove through the slat gap.

These flow states are inherently related to each other, although the delineation of their relationship will require simultaneous measurement of the cove flow and the shedding at the trailing edge for further investigation. This can be accomplished using a two-camera setup, provided that both areas can be illuminated with a single light sheet.

This experimental dataset documents the essential characteristics of the flow field in the slat cove and provides suitable data for the validation of near-field inputs to noise prediction tools. Selected results from this experiment are discussed and compared with unsteady, Reynolds-Averaged Navier-Stokes (URANS) computations for the same configuration in a companion paper by Khorrami, Choudhari, and Jenkins[12].

Acknowledgments

The authors express their appreciation to Mr. Richard White for his assistance in the PIV system setup and Mr. Floyd Backley for making the model modifications.

References

[1]Khorrami, M. R., Singer, B. A., and Lockard, D. P., "Time-Accurate Simulations and Acoustic Analysis of Slat Free-Shear-Layer: Part II," AIAA Paper 2002-2579, 2002.

[2]Choudhari, M., Khorrami, M. R., Lockard, D. P., Atkins, H., and Lilley, G., "Slat Cove Noise Modeling: A Posteriori Analysis of Unsteady RANS Simulations," AIAA Paper 2002-2468, 2002.

[3]Dobryzynski, W., Nagakura, K,, Gehlhar, B., and Buschbaum, A., "Airframe Noise Studies on Wings with Deployed High-Lift Devices," AIAA Paper 1998-2337, 1998.

[4]McGinley, C. B., Anders, J. B., Spaid, F.W., "Measurements of Reynolds Stress Profiles on a High-Lift Airfoil," AIAA Paper 98-2620, 1998.

[5]Storms, B. L., Hayes, J. A., Moriarty, P. J., and Ross, J.C., "Aeroacoustic Measurements of Slat Noise on a Three-Dimensional High-Lift System", AIAA Paper 99-1957, 1999.

[6]Olson, S., Thomas, F. O., and Nelson, R. C., "A Preliminary Investigation into Slat Noise Production Mechanism in a High-Lift Configuration," AIAA Paper 2000-4508, 2000.

[7]Olson, S., Thomas, F. O., and Nelson, R. C., "Mechanisms of Slat Noise Production in a 2D Multi-Element Airfoil Configuration," AIAA Paper 2001-2156, 2001.

[8]Mendoza, J. M., Brooks, T. F., and Humphreys, W. M., "Aeroacoustic Measurements of a Wing/Slat Model," AIAA Paper 2002-2604, June 2002.

[9]Moriarty, P. J. and Heineck, J. T., "PIV Measurements Near a Leading-Edge Slat", Proceedings of the Third International Workshop on PIV, 1999.

[10]Takeda, K., Ashcroft, G. B., Zhang, X., and Nelson, P. A., "Unsteady Aerodynamics of Slat Cove Flow in a High-Lift Device Configuration," AIAA Paper 2001-0706, 2001.

[11]Takeda, K. and Zhang, X., "Unsteady Aerodynamics and Aeroacoustics of a High-Lift Configuration," AIAA Paper 2002-0570, 2002.

[12]Khorrami, M. R., Choudhari, M. M., and Jenkins, L. N., "Characterization of Unsteady Flow Structures Near Leading-Edge Slat: Part II. 2D Computations," AIAA Paper 2004-2802, 2004.

[13]Sellers, W. L. and Kjelgaard, S. O., "The Basic Aerodynamic Research Tunnel – A Facility Dedicated to Code Validation," AIAA Paper 88-1997, May 1988.

[14]Washburn, A. E., "The Effect of Freestream Turbulence on the Vortical Flow over a Delta Wing," Master of Science Thesis, George Washington University, 1990.

[15]Jenkins, L. N., "An Experimental Investigation of the Flow Over a Notchback Automobile Configuration," Master of Science Thesis, George Washington University, 1999.

[16]Klausmeyer, S. M., Papadakis, M., and Lin J. C., "A Flow Physics Study of Vortex Generators on A Multi-Element Airfoil," AIAA Paper 96-0548, January 1996.

[17]Paschal, K., Jenkins, L., and Yao, C., "Unsteady Slat-Wake Characteristics of a High-Lift Configuration," AIAA Paper 2000-0139, January 2000.

[18]Lourenco, L. M. and Krothapalli, A., "True Resolution PIV: A Mesh-Free Second Order Accurate Algorithm," Proceedings of the 10th International Symposium on Application Techniques in Fluid Mechanics, Lisbon, July 2000.

[19]Raffel, M., Willert, C., and Kompenhans, J., *Particle Image Velocimetry – A Practical Guide*, Springer-Verlag, New York, 1998, pp 158-164.

Figures

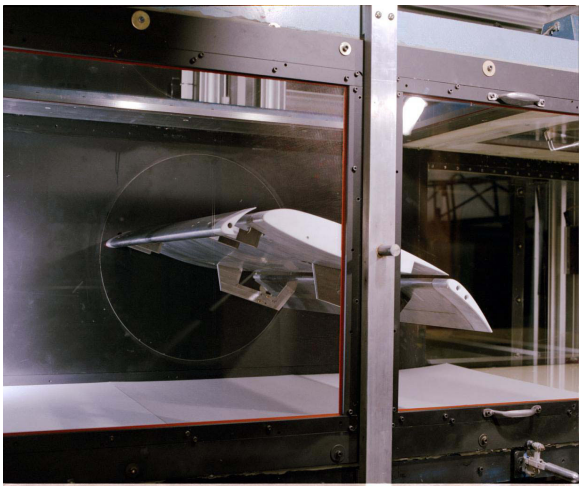

Figure 1: 30P30N airfoil installed in the Basic Aerodynamics Research Tunnel (original bracket design).

Figure 2: 30P30N airfoil with modified "J" brackets.

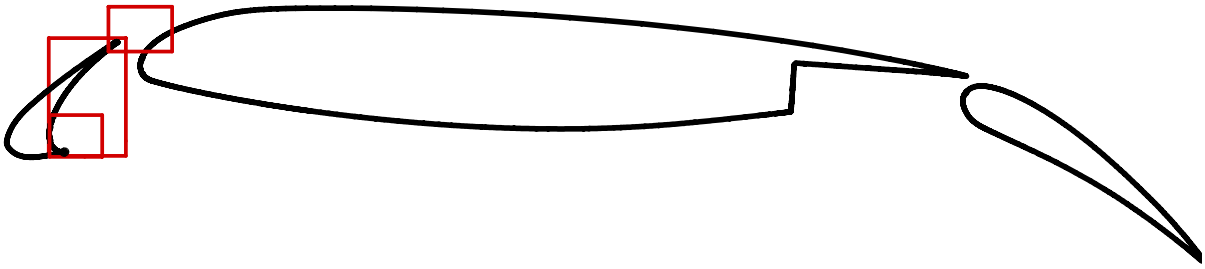

Figure 3: PIV survey locations.

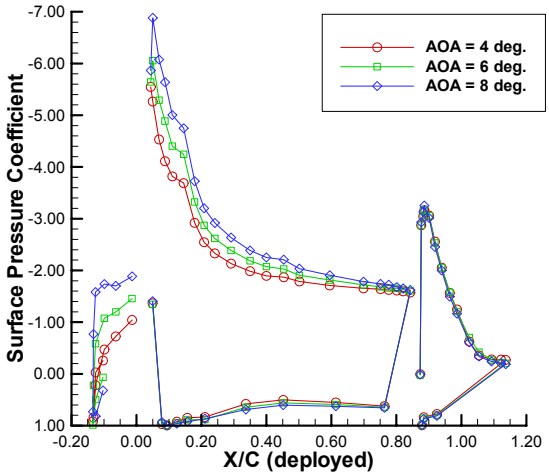

Figure 4: Surface pressure distributions along model centerline.

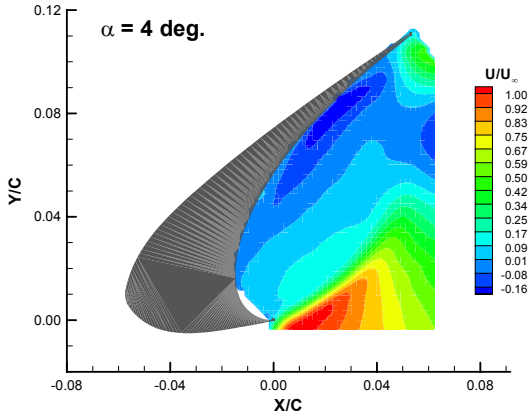

Figure 5a: Mean streamwise velocity.

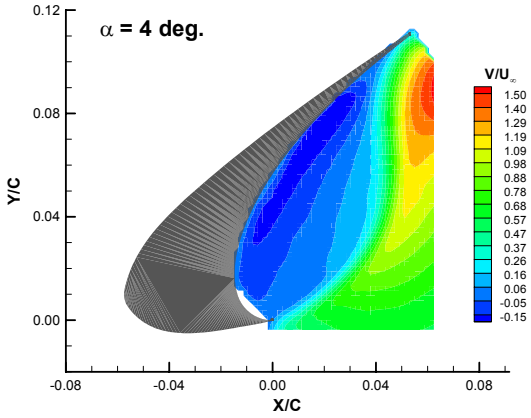

Figure 5b: Mean vertical velocity.

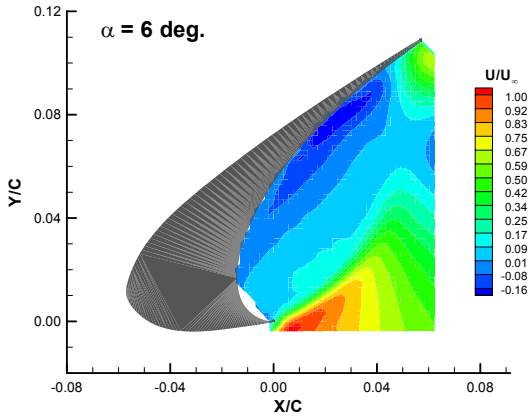

Figure 6a: Mean streamwise velocity.

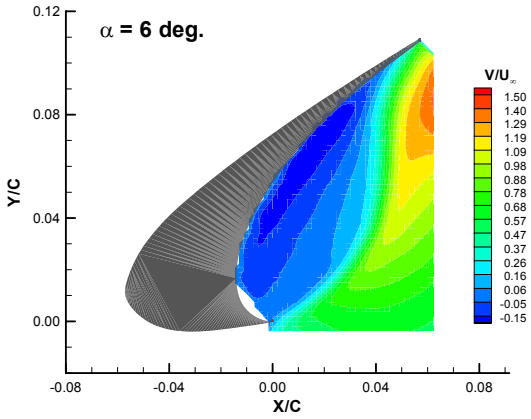

Figure 6b: Mean vertical velocity.

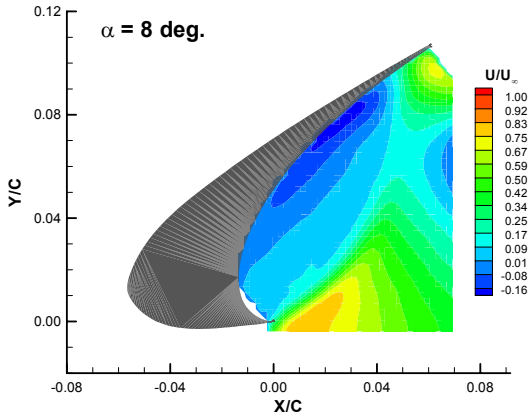

Figure 7a: Mean streamwise velocity.

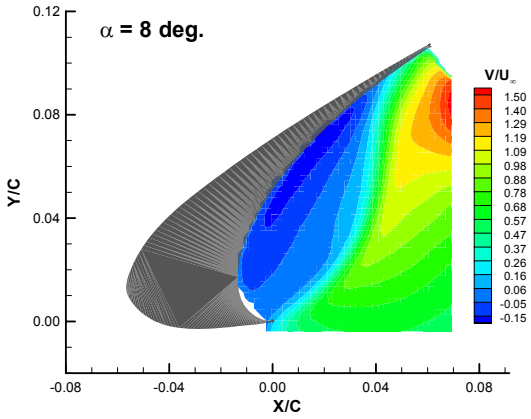

Figure 7b: Mean vertical velocity.

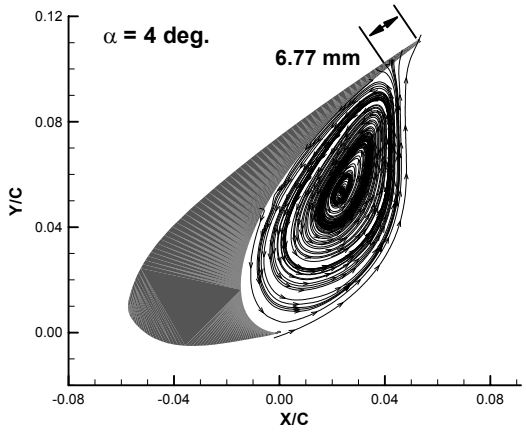

Figure 8: Mean-flow streamlines.

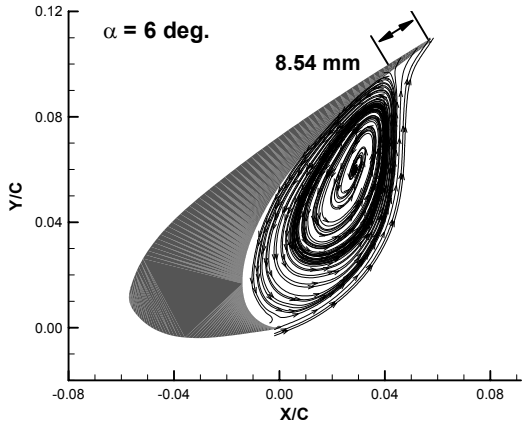

Figure 9: Mean-flow streamlines.

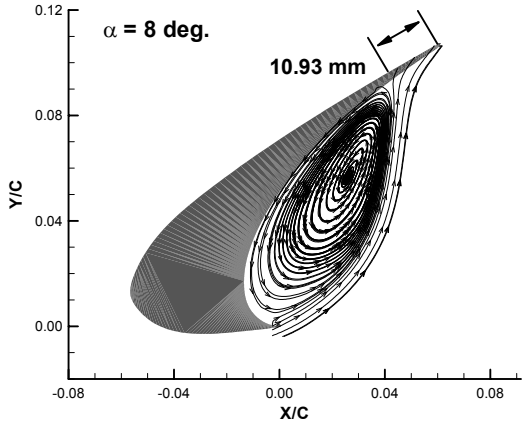

Figure 10: Mean-flow streamlines.

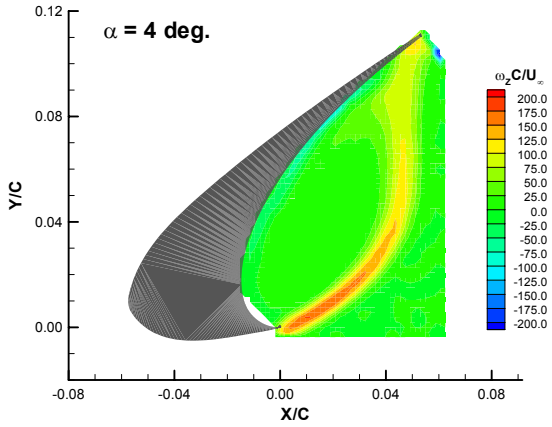

Figure 11a: Mean spanwise vorticity.

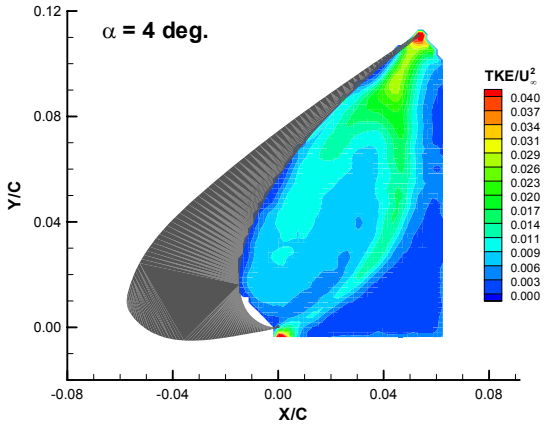

Figure 11b: Turbulent kinetic energy.

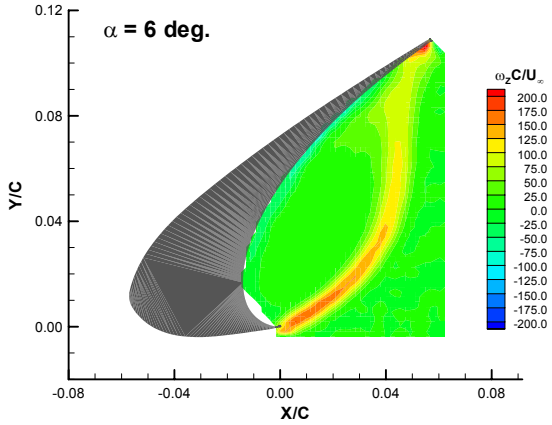

Figure 12a: Mean spanwise vorticity.

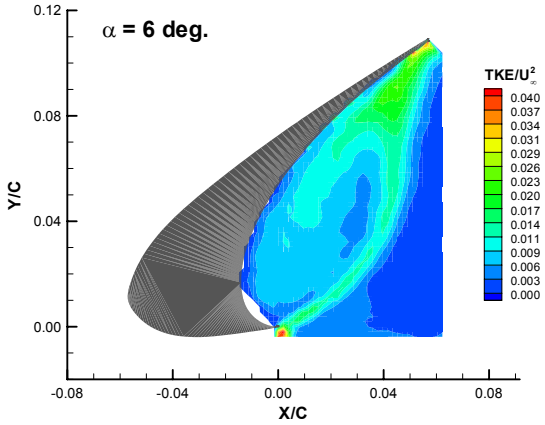

Figure 12b: Turbulent kinetic energy.

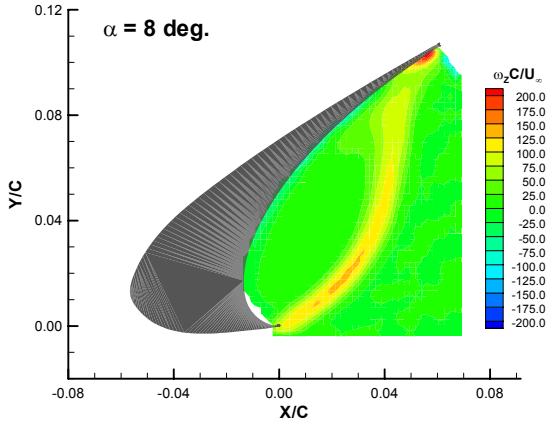

Figure 13a: Mean spanwise vorticity.

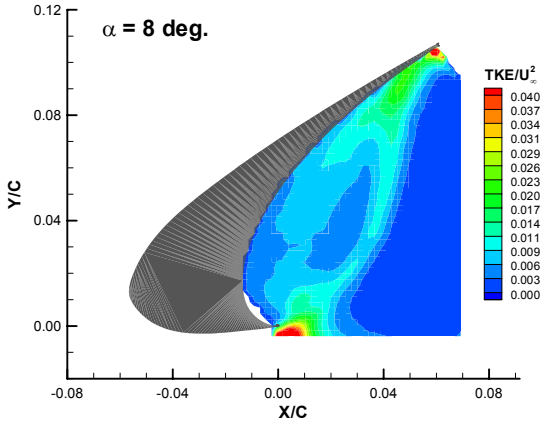

Figure 13b: Turbulent kinetic energy.

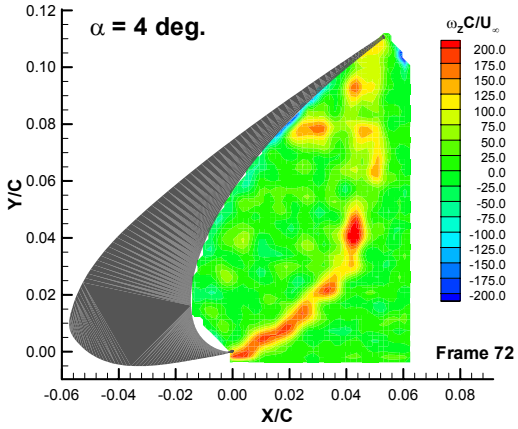

Figure 14a: Instantaneous spanwise vorticity (Cove State 1).

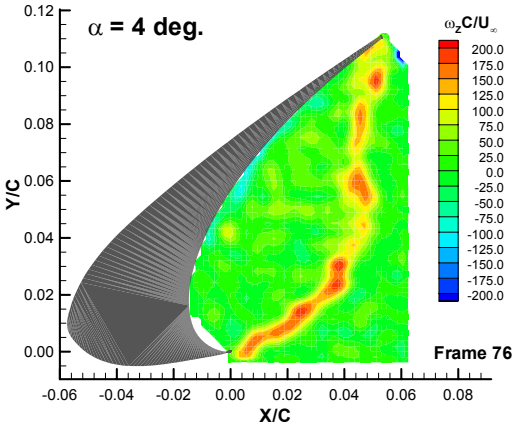

Figure 14b: Instantaneous spanwise vorticity (Cove State 2).

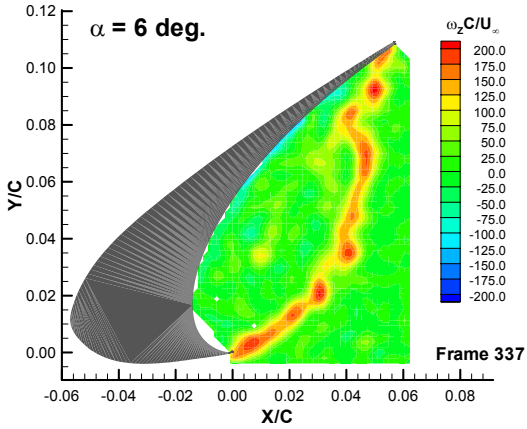

Figure 15a: Instantaneous spanwise vorticity (Cove State 1).

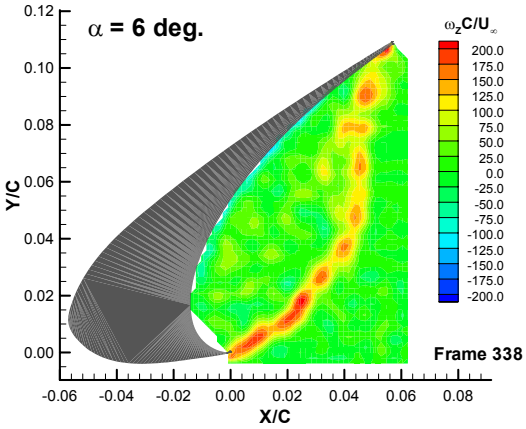

Figure 15b: Instantaneous spanwise vorticity (Cove State 2).

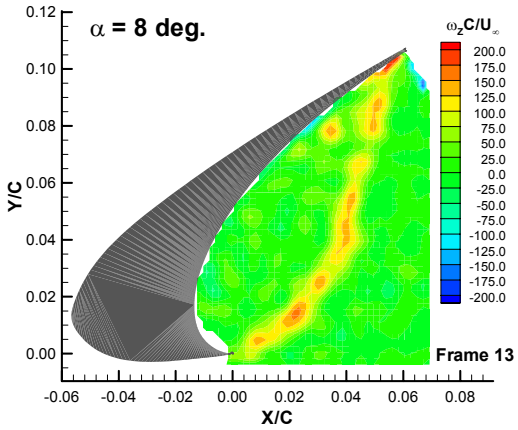

Figure 16a: Instantaneous spanwise vorticity (Cove State 1).

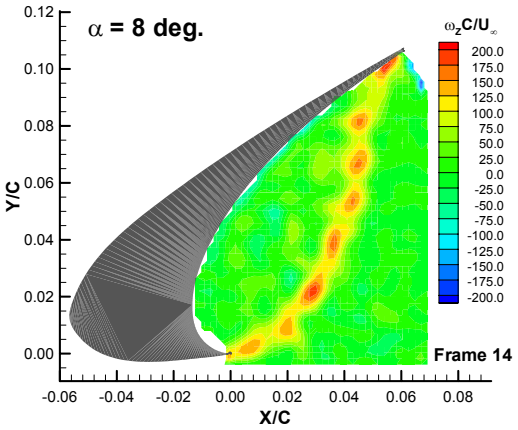

Figure 16b: Instantaneous spanwise vorticity (Cove State 2).

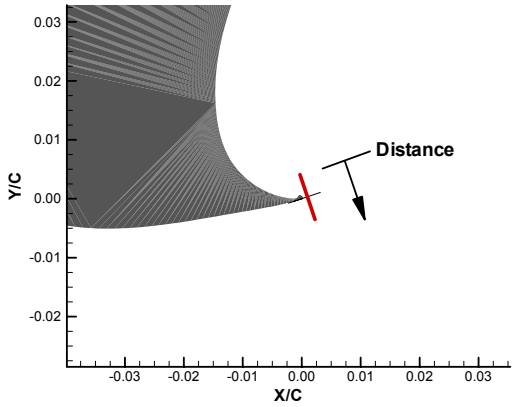

Figure 17: Measurement location for shear layer profiles.

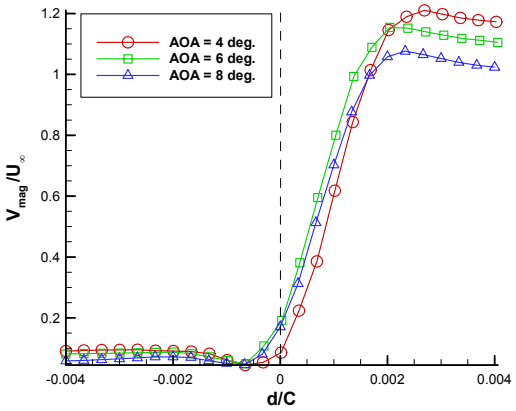

Figure 18: Mean velocity magnitude profiles.

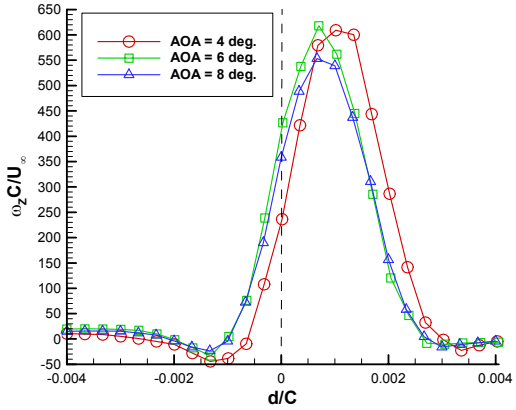

Figure 19: Mean spanwise vorticity profiles.

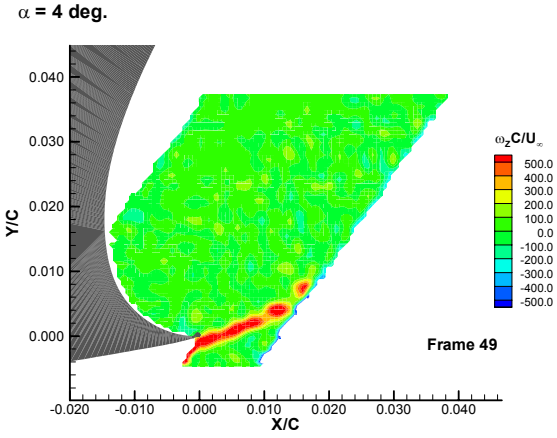

Figure 20: Instantaneous spanwise vorticity.

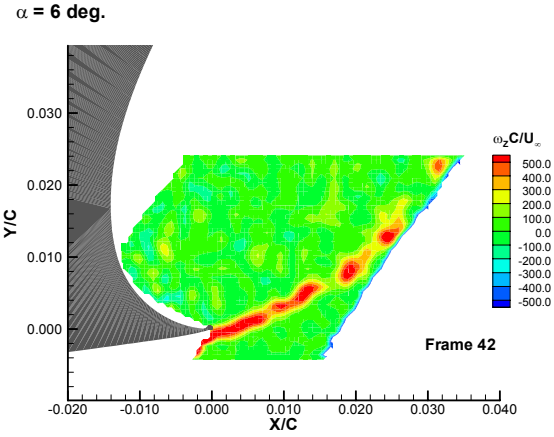

Figure 21: Instantaneous spanwise vorticity.

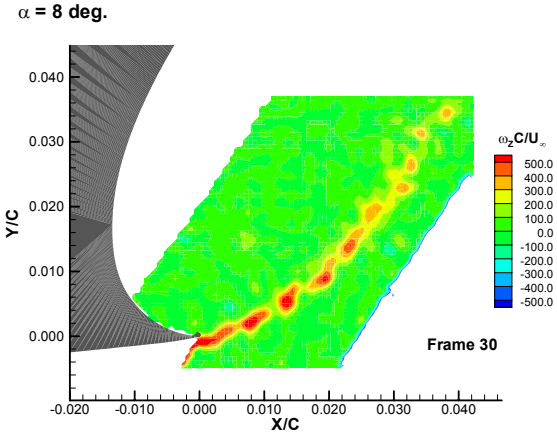

Figure 22: Instantaneous spanwise vorticity.

α = 4 deg.

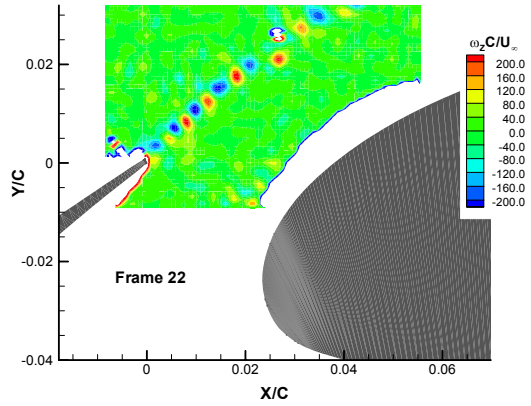

Figure 23a: Instantaneous spanwise vorticity (Slat State 1).

α = 8 deg.

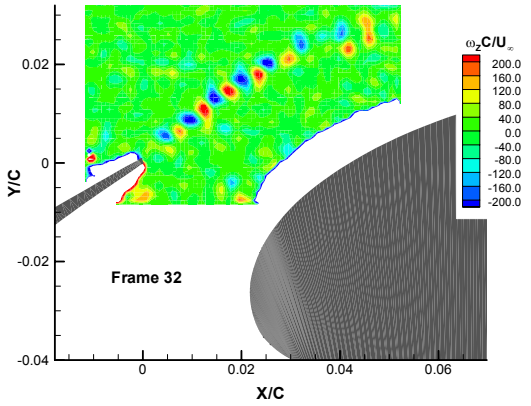

Figure 23b: Instantaneous spanwise vorticity (Slat State 1).

α = 4 deg.

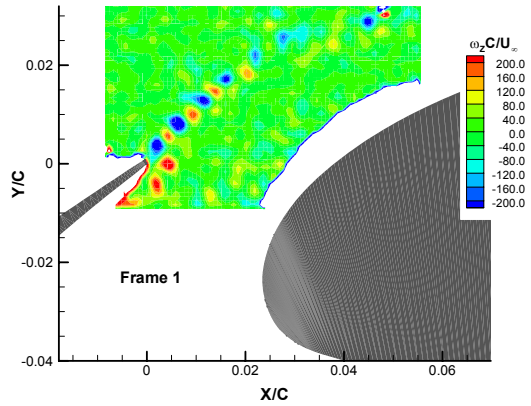

Figure 24a: Instantaneous spanwise vorticity (Slat State 2).

α = 8 deg.

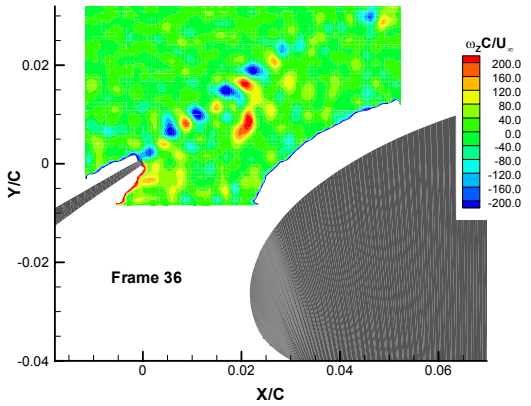

Figure 24b: Instantaneous spanwise vorticity (Slat State 2).

α = 4 deg.

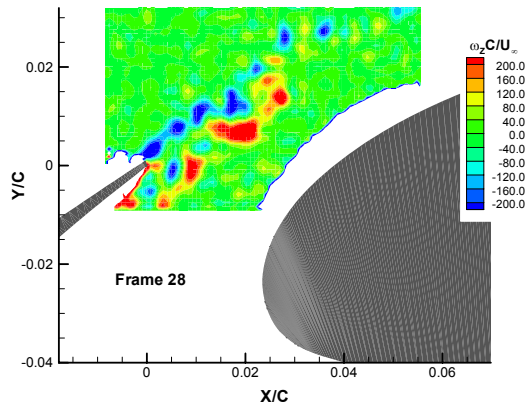

Figure 25a: Instantaneous spanwise vorticity (Slat State 3).

α = 8 deg.

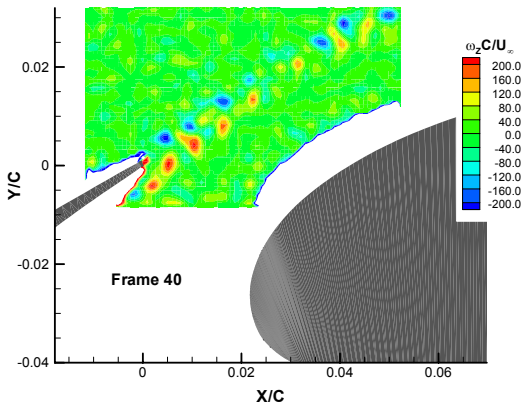

Figure 25b: Instantaneous spanwise vorticity (Slat State 3).

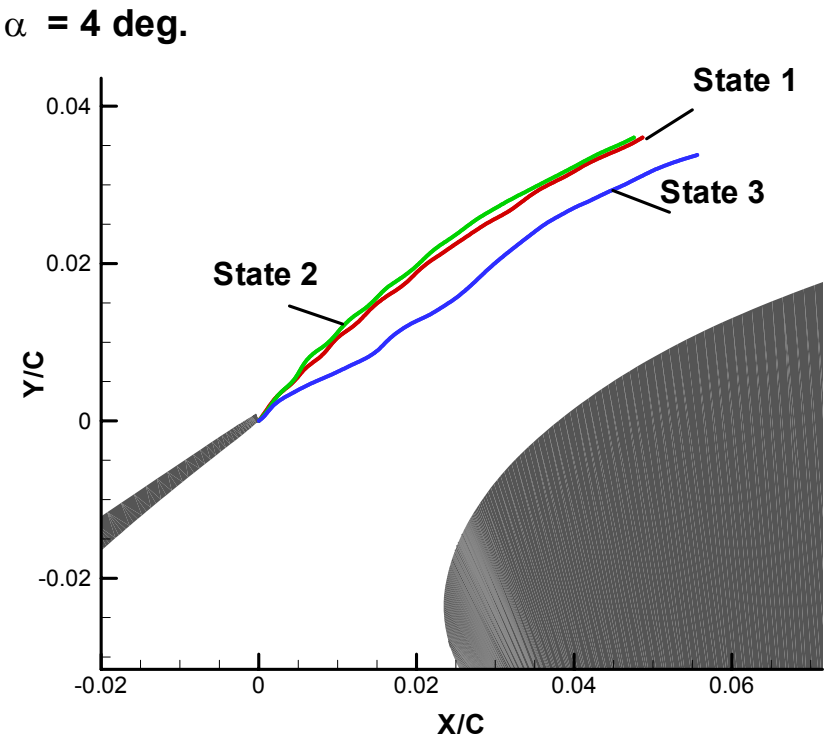

Figure 26: Instantaneous streamlines from the slat trailing edge.

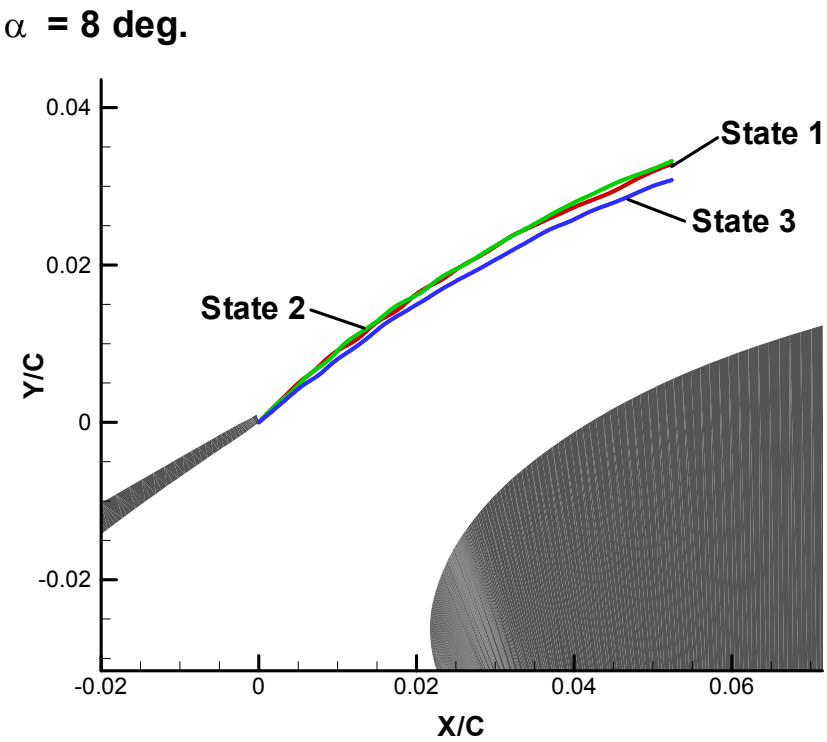

Figure 27: Instantaneous streamlines from the slat trailing edge.